

Heat Capacity of PbS: Isotope Effects

M. Cardona,* R. K. Kremer, R. Lauck, and G. Siegle

*Max-Planck-Institut für Festkörperforschung,
Heisenbergstr. 1, D-70569 Stuttgart, Germany*

J.Serrano

*European Synchrotron Radiation Facility,
Boîte Postale 220, 38043 Grenoble, France*

A.H. Romero

*CINVESTAV, Departamento de Materiales,
Unidad Querétaro, Querétaro, 76230, Mexico*

(Dated: February 1, 2008)

Abstract

In recent years, the availability of highly pure stable isotopes has made possible the investigation of the dependence of the physical properties of crystals, in particular semiconductors, on their isotopic composition. Following the investigation of the specific heat (C_p , C_v) of monatomic crystals such as diamond, silicon, and germanium, similar investigations have been undertaken for the tetrahedral diatomic systems ZnO and GaN (wurtzite structure), for which the effect of the mass of the cation differs from that of the anion. In this article we present measurements for a semiconductor with rock salt structure, namely lead sulfide. Because of the large difference in the atomic mass of both constituents ($M_{\text{Pb}}=207.21$ and ($M_{\text{S}}=32.06$ a.m.u., for the natural isotopic abundance) the effects of varying the cation and that of the anion mass are very different for this canonical semiconductor. We compare the measured temperature dependence of $C_p \approx C_v$, and the corresponding derivatives with respect to (M_{Pb} and M_{S}), with *ab initio* calculations based on the lattice dynamics obtained from the local density approximation (LDA) electronic band structure. Quantitative deviations between theory and experiment are attributed to the absence of spin-orbit interaction in the ABINIT program used for the electronic band structure calculations.

PACS numbers: 63.20.Dj, 65.40.Ba

I. INTRODUCTION

Lead sulfide belongs to the family of the lead chalcogenides (PbS, PbSe, PbTe) which are small bandgap semiconductors that crystallize in the rock salt structure. They differ from the nowadays more commonly encountered tetrahedral semiconductors (e.g. GaAs, ZnO, with zincblende and wurtzite structure, respectively) in that they possess 10 valence electrons per formula unit, as opposed to 8 for the zincblende- and wurtzite-type materials. The lead chalcogenides are found as minerals in nature, bearing the names: galena (PbS), clausthalite (PbSe) and altaite (PbTe). Whereas galena is rather abundant and is found as large, highly perfect crystals, clausthalite and altaite are rare. Some semiconducting properties of PbS have been known since the mid 1800, in particular the rectifying properties of metal-PbS contacts which were used as detectors in early radio receivers¹. The thermoelectric properties of PbS were reported as early as 1865 (Ref. 2). The photoresistive and photovoltaic properties were reported in 1930 (Ref. 3). A number of reviews which summarize the physical properties of PbS have appeared^{4,5}. Particularly interesting is the anomalous dependence of the electronic energy gap on temperature⁶.

The specific heat of PbS was first measured by Eastman and Rodebush above 63 K and subsequently by Parkinson and Quarrington for temperatures between 20 and 270K^{7,8}. Such measurements were extended down to 1K by Lykov and Chernik⁹. Although the typical carrier concentrations of the PbS samples were between 10^{18} and 10^{19} cm⁻³, no evidence of a free carrier contribution to the specific heat was found, except possibly below 2K¹⁰. Thus the measured specific heat represents the contribution of the lattice vibrations vs. temperature, obtained at constant pressure (C_p). Most lattice dynamical calculations, such as those of Elcombe, represent the specific heat measured at constant volume (C_v)¹¹. The difference between C_p and C_v is given by¹²:

$$C_p(T) - C_v(T) = \alpha_v^2(T) \cdot B \cdot V_{mol} \cdot T, \quad (1)$$

where α_v is the temperature dependent thermal expansion coefficient, B the bulk modulus and V_{mol} the molar volume. According to Eq. (1), the difference $C_p - C_v$ increases with increasing T . Replacing standard values of $\alpha_v(T)$, B and V_{mol} found in the literature we obtain from Eq. (1) the difference $C_p - C_v = 0.18$ J/mol K at the highest temperature used in our measurements (~ 280 K). This difference is smaller than typical error bars in our

measurements and will be neglected here. We shall therefore denote the specific heat, either theoretical or experimental, by C_v .

II. THEORETICAL DETAILS

The specific heat of PbS vs. T has been calculated in the harmonic approximation from the vibrational free energy $F(T)$ as obtained with the ABINIT code¹⁴. This code derives the phonon dispersion relations from total energy calculations and uses them to evaluate $F(T)$ with the expression:

$$F(T) = - \int_0^\infty \left(\frac{\hbar\omega}{2} + k_B T \ln[2n_B(\omega)] \right) \rho(\omega) d\omega \quad (2)$$

From Eq. (2) the specific heat is obtained with:

$$C_v = -T \left(\frac{\partial^2 F}{\partial T^2} \right)_v. \quad (3)$$

In Eq. (2), k_B is the Boltzmann constant, n_B the Bose-Einstein factor, and $\rho(\omega)$ the phonon density of states (PDOS). The high frequency cutoff of the latter defines the upper limit of integration in Eq. (2).

The theoretical calculations were performed in the framework of the density functional theory (DFT) by using a local density approximation for the exchange-correlation Hamiltonian as implemented in the ABINIT package. Kohn-Sham orbitals are expanded in plane waves with the use of the Hartwigsen-Goedecker-Hutter pseudopotentials to describe the valence electrons (4 electrons for Pb and 6 electrons for S)¹⁵. A 70 Ry cutoff was used and a Monkhorst Pack grid of $8 \times 8 \times 8$ points was used to describe the electronic properties in the Brillouin zone. Before vibrational calculations were performed, the cell parameter was optimized to a value of 5.808 Å which was used thereafter. The ABINIT program determines the elements of the dynamical matrix by perturbation theory. They were calculated for a $12 \times 12 \times 12$ mesh and then Fourier interpolated to obtain the thermal properties discussed here.

The ABINIT program determines the elements of the dynamical matrix by using perturbation theory. The various isotopic masses used in the calculation were introduced at the level of the dynamical matrix, assuming that the matrix elements of the latter do not depend on those masses. Possible dependence of dynamical matrix elements (i.e. force constants)

on mass can be estimated from Raman and inelastic neutron scattering measurements¹⁶. They are several orders of magnitude smaller than the corresponding isotope mass changes and thus can be neglected for the purpose of the present work.

Under these assumptions and for monatomic crystals (diamond, Ge, Si) all frequencies ω are proportional to $M^{-0.5}$. Because of the appearance of the argument (ω/T) in n_B (Eq. 2), it is possible to relate the derivative of C_v with respect to the isotopic mass M to that with respect to T . The following expression is found¹⁷

$$\frac{d \ln(C_{p,v}/T^3)}{d \ln M} = \frac{1}{2} \left(3 + \frac{d \ln(C_{p,v}/T^3)}{d \ln T} \right). \quad (4)$$

In binary (or multinary) crystals, the masses of the different elements have a different effect on each phonon frequency which, in general, cannot be evaluated with simple arguments. This effect depends on the phonon eigenvectors or, equivalently, on the DOS projected on the atom under consideration¹⁸. As we shall see below, for PbS because of the large difference in the masses of Pb and S, the lattice vibrations are predominantly Pb-like up to 120 cm^{-1} (acoustic phonons). Higher frequency vibrations (optic phonons) are overwhelmingly S-like. The frequency of the acoustic phonons thus should vary, to a good approximation, like the inverse square root of the Pb mass ($M_{\text{Pb}}^{-1/2}$) whereas that of the optic phonons should vary like $M_{\text{S}}^{-1/2}$.

For computational reasons (the limited number of \mathbf{k} -points being sampled) the calculated specific heats are not reliable for T below $\sim 5\text{K}$. A similar low T limit also applies to the experimental data due to the small values of C_v and the limited accuracy of the experimental procedure using sample masses of $\sim 25\text{mg}$ for the isotope enriched samples. $T < 5\text{K}$ corresponds to the Debye limit in which C_v is proportional to (T/θ^3) . This expression enables us to derive for the mass derivatives in the limit $T \rightarrow 0$ the following analytic expressions¹⁹:

$$\frac{d \ln C_v/T^3}{d \ln M_{\text{Pb}}} = \frac{3}{2} \frac{M_{\text{Pb}}}{M_{\text{Pb}} + M_{\text{S}}} = 1.30 \quad \frac{d \ln C_v/T^3}{d \ln M_{\text{S}}} = \frac{3}{2} \frac{M_{\text{S}}}{M_{\text{Pb}} + M_{\text{S}}} = 0.20 \quad (5)$$

The values given in Eqs. (5) can be used to extrapolate those obtained at 5K to $T \rightarrow 0$.

In order to achieve convergence of the heat capacity and its logarithmic derivatives with respect to M_{Pb} and M_{S} a grid of $80 \times 80 \times 80$ \mathbf{q} points in the irreducible Brillouin zone was used for the evaluation of the PDOS and the thermodynamic properties. The number of \mathbf{q} points used in the integrations (e.g., Eq. 2) is particularly important for the convergence of the

calculations of the mass derivatives at low temperature. These calculations were performed by evaluating the differences of C_v for two different lead and sulfur pairs of isotopes. Below 5K, the calculated derivatives depended strongly on the pair of isotopes and the sample chosen. We kept only the values for $T \rightarrow 0$ as given by Eq. 5

III. LATTICE DYNAMICS: DISPERSION RELATIONS AND DENSITY OF PHONON STATES

Figure 1 displays the phonon dispersion relations of natural PbS obtained from the *ab initio* electronic band structure using the procedure described above (solid lines). Experimental points obtained by inelastic neutron scattering (INS)¹¹ are denoted by diamonds. Of particular interest is the large LO - TO splitting which, by virtue of the Lyddane-Sachs-Teller relation²⁰, indicates a large value of the low-frequency dielectric constant ($\epsilon(0) \sim 180$, $\epsilon(\infty) \sim 18$) which is related to the nearly ferroelectric character of PbTe²¹.

The INS points in Fig. 1 agree reasonably well with the calculated dispersion relations except for the TO modes along the Σ and the Δ directions. Previous calculations were of a semi-empirical nature with parameters adjusted to fit the INS results^{11,22}. It is therefore not surprising that the agreement between the calculated dispersion relations and the INS results is somewhat better than that of Fig. 1.

We conjecture that the discrepancies between theory and experiments displayed in Fig. 1 may be due to the lack of the spin-orbit interaction contribution in the corresponding LDA Hamiltonian. This conjecture is supported by recent *ab initio* calculations of the phonon dispersion relations of bismuth performed with and without spin-orbit interaction²³. *ab initio* electronic band structure calculations which include spin-orbit coupling have been recently performed for PbS, PbSe, and PbTe but, to our knowledge, they have not been used to derive the phonon dispersion relations. *Ab initio* calculations of the LO and TO frequencies at $\mathbf{q}=0$ have been reported for PbTe²⁵.

The TO bands of Fig. 1 are nearly dispersionless along Σ and Δ . This fact suggests phonon modes in which the lead and the sulfur vibrations are only weakly coupled, a conjecture which is confirmed by the calculated phonon eigenvectors and also by the PDOS displayed in Fig. 2 as projected on the lead (predominant below 120 cm^{-1}) and the sulfur (predominant above 120 cm^{-1}) eigenvectors. The van Hove singularities of the TA modes at

the L and X points are responsible for the sharp, Pb-like spike seen at $\sim 50 \text{ cm}^{-1}$ (cf. Fig. 2), whereas the flat regions of the TO bands are responsible for the much lower peak found at $\sim 130 \text{ cm}^{-1}$.

IV. EXPERIMENTAL PROCEDURE

The preparation and some properties of the PbS samples are described in Ref. 26. Two types of samples with the natural isotopic composition ($M_{\text{Pb}} = 207.21 \text{ a.m.u.}$, $M_{\text{S}} = 32.05 \text{ a.m.u.}$) were used. One was a piece of natural galena (from Creede, CO, USA, 16 mg) whereas the others were pieces of the same size taken from the synthetic ingots used in Ref. 26. We also measured a piece of the $^{\text{nat}}\text{Pb}^{34}\text{S}$ of Ref. 26 and a piece from an ingot prepared in the same way with the isotopic composition $^{208}\text{Pb}^{\text{nat}}\text{S}$. All samples were p-type (as determined from the sign of the thermoelectric power), the natural sample had a carrier concentration of $2 \times 10^{17} \text{ cm}^{-3}$ whereas the synthetic ones had carrier concentrations around 10^{18} cm^{-3} (as determined from the infrared plasma edge, see Ref. 26).

The synthetic ingots were prepared by first reacting the corresponding pure elements and then subliming the compound in an argon atmosphere as described in detail in Ref. 26.

The heat capacities were measured between 5 and 280K with a PPMS system (Quantum Design, 6325 Lusk Boulevard, San Diego, CA.) as described in Ref. 19. All natural samples measured gave the same results within error bars.

V. EXPERIMENTAL VS. THEORETICAL RESULTS

Figure 3 shows the specific heat measured for our $^{\text{nat}}\text{Pb}^{\text{nat}}\text{S}$ samples for T between 1.8 and 270K and that reported in Ref. 8 for T between 20 and 260 K. The solid line represents the results of our *ab initio* calculation. Whereas the two sets of experimental data agree within error bars (the widths of the symbols in the plot), the calculated curve falls slightly below the measurements, especially around 80K. The sign of this deviation corresponds to calculated phonon frequencies lying above the experimental ones, as is the case for the TO modes in Fig. 1. Notice that at temperatures above 280K C_v tends to the Petit and Dulong value ($C_v \sim 49 \text{ Joule/mole K}$)²⁷.

In order to be able to read the low temperature data of Fig. 3, which according to Debye's

law should be proportional to T^3 , we display in Fig. 4 the quantity $C_v(T)/T^3$. This figure reveals that the region of validity of Debye's law is rather small ($T < 3\text{K}$). This follows from the flattening of the TA dispersion relations with increasing q . Figure 4 also shows that the calculated value of C_v/T^3 at its maximum ($T_{max} \sim 11\text{K}$) is about 23% lower than the measured one. This discrepancy can be assigned to that of the calculated TO frequencies (Fig. 1) which has already been attributed to the lack of spin-orbit interaction in the band structure calculations. We recall that in the case of bismuth a similar discrepancy is found when the *ab initio* calculations are performed without spin-orbit coupling²³.

Using Debye's theorem²⁸, Fig. 4 can be recast into a form which exhibits the temperature dependence of an equivalent $\theta_D(T)$ (Fig. 5). This figure, which includes calculated¹¹ as well as experimental data, reveals a value of θ_D equal to 210 K in the $T \rightarrow 0$ limit. $\theta_D(T)$ decreases to a minimum of 135 K at $\sim 20\text{K}$.

$\theta_D(T)$ saturates at $\theta_D \sim 230$ K for $T > 230\text{K}$. Note that in spite of the large scatter in our experimental points, the agreement between theory and experiment is rather good, except in the region around 75 K where a difference of about 1% appears. In order to get a feeling for the dependence of the results of Fig. 4 on isotopic masses, especially around the maximum, we plot in Fig. 6a and 6b *ab initio* calculations for different sulfur (Fig. 6a) and lead (Fig. 6b) isotopes. We note that a 2% variation in M_{Pb} results in a 3% variation in C_v/T^3 whereas a 3% variation in M_{S} results in a 0.5% variation of C_v/T^3 . This reveals a low sulfur content in the eigenvalues of the acoustic modes as already discussed in connection with Fig. 2.

Figure 7 displays the change in C_v/T^3 measured and calculated for a change of one a.m.u. in the mass of Pb in PbS. Below 6K, the calculations (and also the measurements) yield unreliable results. Correspondingly, the calculated curve has been extrapolated to the value calculated for $T \rightarrow 0$ using Eqs. 5 and the Debye limit for C_v ($C_v/T^3 \sim 3\mu\text{J/mol K}^4$). The maximum in both, experimental and calculated data occurs for $T \sim 12$ K. Note that the larger isotope mass yields a larger value of C_v/T^3 .

Figure 8 shows experimental and calculated results similar to those in Fig. 7 but obtained for a change of 2 a.m.u. in M_{S} . The calculated curve displays a maximum at 35 K. The measured points scatter markedly around this temperature but, on the average, they are also compatible with the existence of a maximum at 35 K. Below $\sim 10\text{K}$ both sets of data become unreliable. We have also extrapolated the calculated curve to join the value predicted with

Eqs. 5 and the Debye law.

VI. DISCUSSION

As shown in Figs. 3 and 4 our calculations, based on phonon dispersion relations obtained from *ab initio* electronic band structures, reproduce reasonably well the experimental results. The discrepancy which appears at the maximum of Fig. 4 can be attributed to the lack of spin-orbit interaction in the otherwise relativistic Hamiltonian used for the *ab initio* electronic calculations. The peak in the $\Delta C_v/T^3$ of Fig. 7 occurs at 12 K, a temperature about one-third that of the peak seen in Fig. 8. The ratio of both temperatures approximately equals the square root of the corresponding masses. This fact allows us to assign the peak in Fig. 7 to vibrations of lead atoms and that in Fig. 8 to those of sulfur atoms, in agreement with the assignment of the structures in the PDOS of Fig. 2 below and above 120 cm^{-1} . The Pb-like PDOS of Fig. 2 shows a sharp peak at 55 cm^{-1} ($\sim 80\text{K}$ in temperature units) which has been discussed in Sect. III. The S-like PDOS spreads over a broad band with a peak at 133 cm^{-1} ($\sim 196\text{ K}$). The ratio of the temperatures of these two peaks to those of the maxima in Figs. 7 and 8 is ~ 6 . By modeling the two peaks in the PDOS with single harmonic oscillators (Einstein model) it is possible to calculate peaks in $\Delta C_v/T^3$ at temperatures close to those displayed in Figs. 7 and 8. For simplicity, let us consider an Einstein oscillator with a frequency equivalent to 100K which is inversely proportional to the square root of its mass. The logarithmic derivative of the corresponding specific heat with respect to the mass is

$$\frac{d(C_v/T^3)}{d \ln M} \sim \frac{0.5}{100T^2} \frac{d^2}{dT^2} \frac{1}{(e^{\frac{100}{T}} - 1)} = -T^{-6} e^{\frac{100}{T}} \frac{e^{\frac{100}{T}}(T - 50) - T - 50}{(e^{\frac{100}{T}} - 1)^3}. \quad (6)$$

Calculations based on Eq. (6) are plotted in Fig. 9, with the vertical axis in arbitrary units.

The ratio of the Einstein oscillator temperature T_E to that of the peak in Fig. 9 is $100/16=6.25$ and is independent of T_E . This ratio agrees rather well with the value obtained from Figs. 7 and 2 (6.25) for the derivative vs. M_{Pb} and for that vs. M_{S} from Figs. 8 and 2 (6.1). It is interesting to compare these ratios with those obtained for two rather similar materials: ZnO (Ref. 19) and GaN (Ref. 12). For ZnO one obtains the ratio 7.3 for the M_{Zn} derivative and 5.1 for the M_{O} derivative, whereas in the case of GaN one finds 6.5 for

the M_{Ga} derivative and 3.5 for the M_{N} derivative.

We have already mentioned in Sec. II that for monatomic crystals the mass derivative of the specific heat can be obtained from the corresponding temperature derivative by using Eq. (4)¹⁷. This equation cannot be used for crystals containing several different atoms per primitive cell such as PbS, a fact which becomes obvious when one considers that there is only one temperature derivative but two (or more) independent mass derivatives. It was shown, however, in Ref. 12 (for GaN) and Ref. 19 (for ZnO) that the sum of the corresponding cation and anion mass derivatives equals the result obtained with Eq.(4) from the temperature derivative. Figure 10 demonstrates that the same property applies to PbS. This figure includes the results obtained by replacing into Eq.(4) the experimental as well as the *ab initio* calculated temperature derivatives. The figure also includes the two appropriate mass derivatives and their sum (all from the *ab initio* calculations). Some difference appears between the latter and the curve obtained from the measured temperature derivative near the maximum at about 20K. We believe that their origin lies in experimental and computational errors at these rather low temperatures and also in the neglect of spin-orbit coupling in the *ab initio* calculations.

VII. CONCLUSIONS

We have investigated experimentally and theoretically (*ab initio*) the specific heat of PbS and its derivatives with respect to the masses of the two constituents. Reasonable agreement is found between experiment and calculations, quantitative differences having been attributed to the absence of spin-orbit interaction in the latter. The mass derivatives vs. T exhibit maxima at about 12 K for lead and 33 K for sulfur. The large difference in the masses of both constituents allows us to separate these maxima and to relate them to corresponding maxima in the PDOS. The frequency of the latter is about six times larger than that of the former: a simple model, based on a single Einstein oscillator, has been proposed to account for this factor. Qualitatively similar ratios have been found in recent years for ZnO and GaN, two materials for which the ratio of cation to anion mass is not as large as for PbS. Note that the Einstein oscillator curve of Fig.9 can be used, by adjusting the oscillator frequency and the vertical scale, to give a rather good representation of the experimental data (and the calculations) of Figs. 7 and 8.

By inverting the integral equation relating the specific heat and its derivatives to the components of the phonon eigenvectors on the two (or more) constituent atoms, it should be possible to obtain the corresponding projected densities of states from experimental data. Because of the large error bars in some of our measured points, however, we have not implemented this procedure. *ab initio* calculations of the projected PDOS have led us to the conclusion, that below 120 cm^{-1} , the eigenvectors are to a large degree lead -like, whereas above this frequency they are almost completely sulfur-like.

In order to remove remaining discrepancies between theory and *ab initio* calculations it should be interesting to modify the ABINIT code so as to include spin-orbit coupling in the phonon calculations. Spin-orbit coupling is only included, in the ABINIT version available to us for calculating the specific heat, for monatomic materials such as bismuth^{23,29}. A procedure to include spin-orbit splitting in lattice dynamical calculations with ABINIT would be highly desirable in order to ascertain the contributions in the phonon dispersion and thermodynamical properties in lead chalcogenides, among other multinary semiconductors.

Acknowledgments

We thank L. Wirtz and O. Kilian for very fruitful discussions and for making available to us unpublished results on the phonon dispersion of lead chalcogenides.

* Corresponding author: E-mail M.Cardona@fkf.mpg.de

¹ F. Braun, Ann. Phys. Chem., **153**, 556 (1874)

² J. Stefan, Pogg. Annalen d. Physik **124**, 632 (1865)

³ B. Lange, Naturwiss. **18**, 917 (1930) ; Z. Phys. **31**, 968 (1930)

⁴ Yu. I. Ravich, B.A. Efimova and I.A. Smirnov, Semiconducting Lead Chalcogenides (Plenum Press, New York, 1970)

⁵ R. Dalven, Solid State Physics Vol. 28 (Academic Press, N.Y., 1973), p.179

⁶ W. Paul and R.V. Jones, Proc. Phys. Soc. London, **B66**, 194 (1953); H.Y. Lian et al., Phys. Rev. **B73**, 233202 (2000)

⁷ E.D. Eastman and W.H. Rodebush, J. Am. Chem. Soc. **40**, 489 (1918)

- ⁸ D.H. Parkinson and J.E. Quarrington, Proc. Phys. Soc. **A67**, 573 (1954)
- ⁹ S.N. Lykov and I.A. Chernik, Sov. Phys. Solid State **24**, 1755 (1982)
- ¹⁰ P.H. Keesom and G.M. Seidel, Phys Rev. **113**, 33 (1959)
- ¹¹ M.M. Elcombe, Proc. Roy. Soc. (London) **A300**, 210 (1967)
- ¹² R.K. Kremer, M.Cardona, E.Schmitt, J.Blumm, S.K. Estreicher, S. Sanati, M. Bockowski, I. Grzegory, T.Suski, and A. Jezowski, Phys. Rev. B **72**, 075209 (2005)
- ¹³ Landoldt-Börnstein Tables. new series Group III Vol 17f, G. Nimtz ed. (Springer, Berlin, 1983) p. 155
- ¹⁴ The ABINIT code results from a common project of the Universit Catholique de Louvain, Corning Incorporated, and other collaborators (URL: <http://www.abinit.org>)
- ¹⁵ C. Hartwigsen, S. Goedecker, and J. Hutter, Phys. Rev. B **58**, 3641 (1998)
- ¹⁶ M.Cardona and M.L.W. Thewalt, Rev. Mod. Phys. **77**, 1173 (2005)
- ¹⁷ M.Sanati, S.K. Estreicher, and M.Cardona, Solid State Commun., **131**, 229 (2004)
- ¹⁸ J. Menendez, J.B. Page, and S. Guha, Phil. Mag. B **70**, 651 (1994)
- ¹⁹ J. Serrano, R.K. Kremer, M. Cardona, G. Siegle, A.H. Romero, and R.Lauck, Phys. Rev. B **73**, 094303 (2006)
- ²⁰ R.H. Lyddane, R.G. Sachs, and E. Teller, Phys. Rev. **59**, 673 (1941)
- ²¹ G. Grabecki *et al.*, Physica E **35**, 332 (2006)
- ²² K.S. Upanhyaya, M. Yadav and G.K. Upadhyaya, Phys. stat. sol. (b) **922**, 1129 (2002)
- ²³ L.E. Díaz-Sánchez, A.H. Romero, and X. Gonze., unpublished. Note that the crystal structure of bismuth is rather similar to that of PbS. The atomic potential of Bi is also similar to that of Pb, in particular its spin-orbit coupling.
- ²⁴ E.A. Albanesi, E.L. Peltzer y Blanca, and A.G. Petukhov, Computational Materials Science **32**, 85 (2005)
- ²⁵ N.E. Zein, V.I. Zinenko and A.S. Fedorov, Physics Letters A **164**, 115 (1992)
- ²⁶ R. Sherwin, R.J.H. Clark, R.Lauck, and M. Cardona, Solid State Commun. **134**, 565 (2005)
- ²⁷ A.T Petit and P.L. Dulong, Ann. Chim. Phys. **10**, 395 (1819)
- ²⁸ P. Debye, Ann. d. Physik, **39**, 789 (1912)
- ²⁹ E.D. Murray, S. Fahy, D. Prendergast, T. Ogitsu, D.M. Fritz, and D.A. Reis , Phys. Rev. B in press.

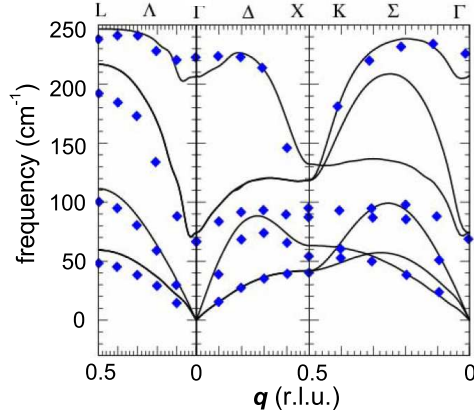


FIG. 1: (color online) Phonon dispersion relations of PbS assuming the natural isotope compositions for Pb and S obtained from the ab initio electronic band structure using the ABINIT code (black solid line). Experimental points obtained by inelastic neutron scattering measurements are denoted by (blue) diamonds¹¹. Note that the TO band is considerably higher than the experimental data points around the X and K points, a fact which is attributed in the text to the lack of spin-orbit interaction in the ABINIT code used¹⁴.

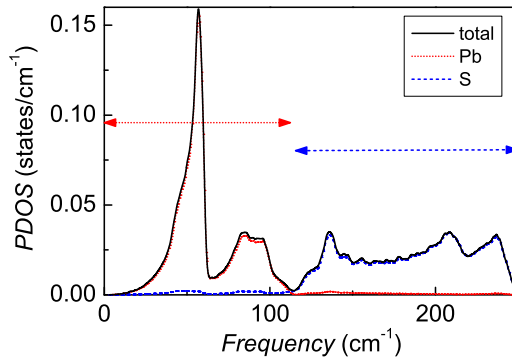


FIG. 2: (color online) Phonon density of states (PDOS) of PbS (total, black solid line) obtained from the dispersion relations of Fig. 1 and its components projected on the Pb and S atoms (red dots and blue dashes). The horizontal arrows indicate the regions of predominant Pb and S contributions, respectively. For frequencies below (above) 120 cm^{-1} the sulfur (lead) component is extremely small (less than 1%).

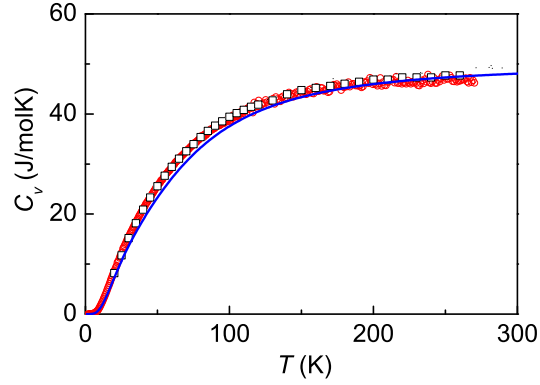


FIG. 3: (color online) Experimental molar specific heat of PbS (galena, natural isotope composition of Pb and S, respectively (red circles). Also shown is the specific heat calculated from the PDOS of Fig. 2 (blue solid line) and the data by Parkinson (galena, Ref. 8).

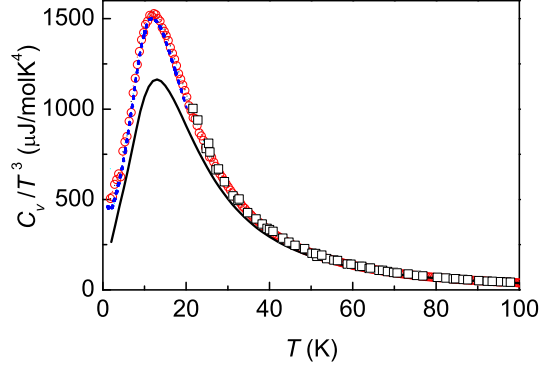


FIG. 4: (color online) Temperature dependence of C_v/T^3 as obtained from the ABINIT calculation (lower (black) solid curve) and measured by Lykov and Chernik (Ref. 9) (upper dashed (blue) curve), by Parkinson (Ref. 8) (black squares), and by us (red circles). The difference between the measurements and the ABINIT calculations is attributed to the lack of spin-orbit interaction in the latter.

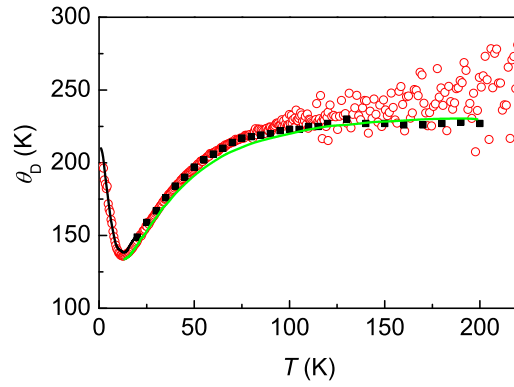


FIG. 5: (color online) Effective Debye temperature $\theta_D(T)$ (see text) of PbS. Our data for PbS (natural isotope composition for Pb and S, respectively, are displayed by (red) circles. Parkinson's data (Ref. 8) by (black) squares, the data reported by Lykov and Chernik (Ref. 9) are represented by the (black) solid line. The (green) solid curve represents the results of semiempirical calculations by Elcombe (Ref. 11).

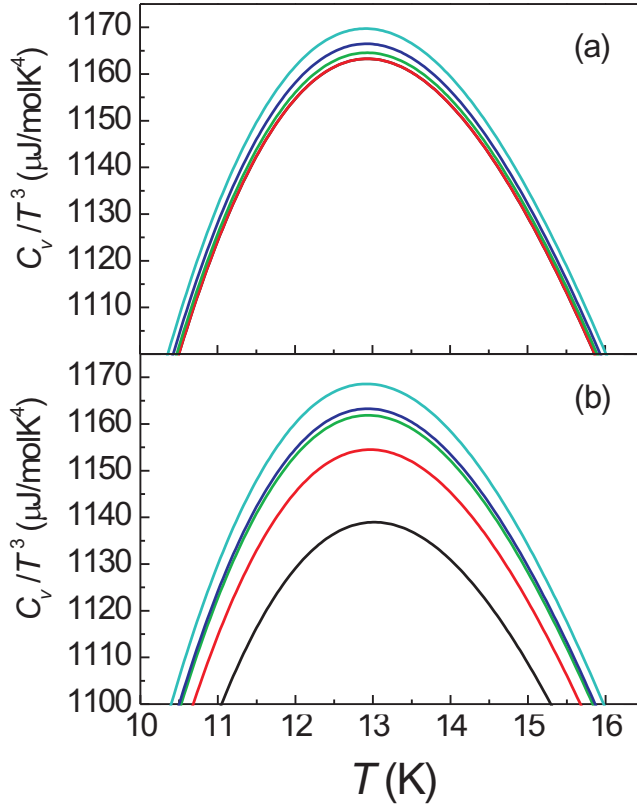


FIG. 6: (color online) ABINIT calculations of C_v/T^3 for PbS with various isotope compositions. (a) $^{\text{nat}}\text{Pb}^n\text{S}$ with (from top to bottom) $n=36, 34, 33, \text{nat}, 32$ a.m.u. (note that the curves for $^{\text{nat}}\text{Pb}^{\text{nat}}\text{S}$ and $^{\text{nat}}\text{Pb}^{32}\text{S}$ lie on top of each other). The superscript nat refers to the natural isotope abundance of S which corresponds to an atomic mass of 32.06 a.m.u. (b) $^m\text{Pb}^{\text{nat}}\text{S}$ with (from top to bottom) $m=208, \text{nat}, 207, 206, 204$ a.m.u. The superscript nat refers to the natural isotope abundance of Pb which corresponds to an atomic mass of 207.21 a.m.u. The isotope effects are much smaller in (a) than in (b), as corresponds to the low sulfur content of the lower frequency eigenvectors.

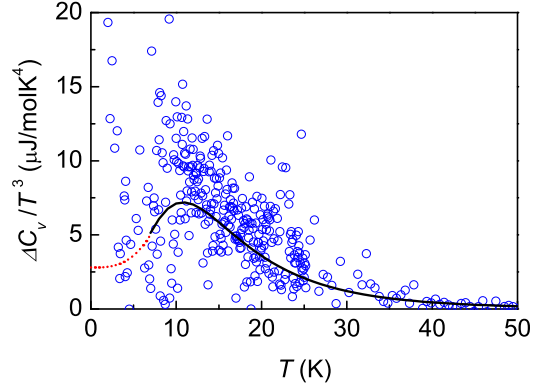


FIG. 7: (color online) $\Delta C_v/T^3$ difference for two samples with natural sulfur and two different lead isotopic compositions (natural and $M_{\text{Pb}} = 208$ a.m.u.). The (blue) circles represent experimental points, the (black) solid curve calculations which are not reliable below $\sim 6\text{K}$. The (red) dotted curve represents an extrapolation of the calculated curve for $T \rightarrow 0$ according to Eq. 5.

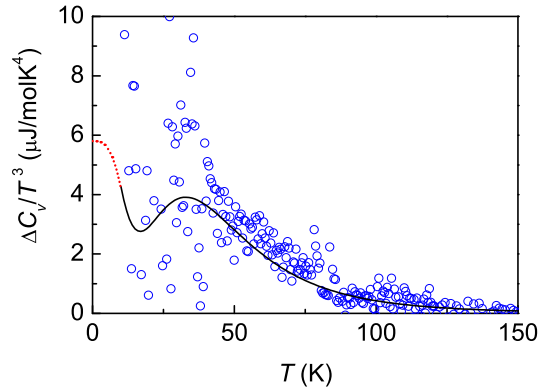


FIG. 8: (color online) $\Delta C_v/T^3$ difference for two samples with natural Pb and two different sulfur isotopic compositions (natural and $M_{\text{S}} = 34$ a.m.u.). The (blue) circles represent experimental points, the (black) solid curve calculations which are not reliable below $\sim 6\text{K}$. The (red) dotted curve is an extrapolation of the calculated curve for $T \rightarrow 0$ using Eq. 5.

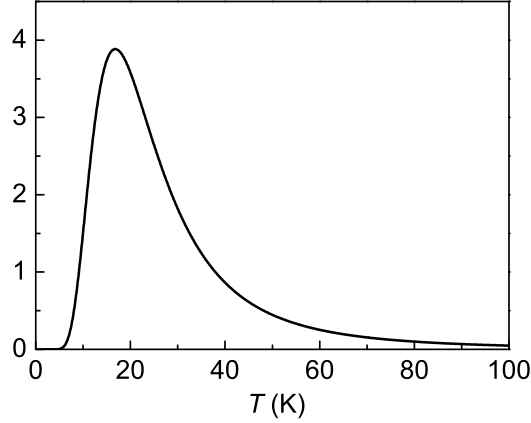


FIG. 9: Einstein oscillator model for the isotope effects of Figs. 7 and 8. The curve was obtained with Eq. (6) which assumes, for simplicity, an Einstein temperature of 100K. The temperature of the peak is 16.5K. The ratio of the Einstein to the peak temperature is, ≈ 6 , independent of the Einstein temperature.

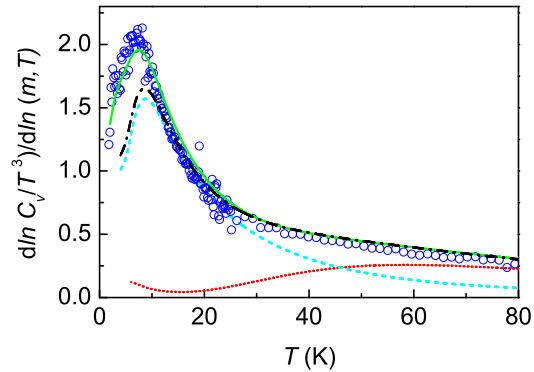


FIG. 10: (color online) The (blue) circles represent the derivative with respect to temperature, $d \ln(C_v/T^3)/d \ln T$ of the specific heat of of PbS (galena). The data points were smoothed by averaging five neighbor data points on either side (adjacent averages). The (green) solid curve shows the r.h.s. of Eq. (4), the (magenta) dashed and (red) dotted curves the derivatives with respect to the mass, $d \ln(C_v/T^3)/d \ln M$, with M being the mass of either lead or sulphur, respectively. The (black) dashed-dotted solid curve is the sum of these derivatives (l.h.s. of Eq. (4)). Note that above 40K the (green) solid and the (black) dashed-dotted curves lie on top of each other.